

The Gaia FGK benchmark stars ^{★,★★}

High resolution spectral library

S. Blanco-Cuaresma^{1,2}, C. Soubiran^{1,2}, P. Jofré^{1,2,3}, and U. Heiter⁴

¹ Univ. Bordeaux, LAB, UMR 5804, F-33270, Floirac, France.

² CNRS, LAB, UMR 5804, F-33270, Floirac, France

³ Institute of Astronomy, University of Cambridge, Madingley Road, Cambridge CB3 0HA, U.K.

⁴ Department of Physics and Astronomy, Uppsala University, Box 516, 75120 Uppsala, Sweden

March 26, 2015

ABSTRACT

Context. An increasing number of high-resolution stellar spectra is available today thanks to many past and ongoing spectroscopic surveys. Consequently, numerous methods have been developed to perform an automatic spectral analysis on a massive amount of data. When reviewing published results, biases arise and they need to be addressed and minimized.

Aims. We are providing a homogeneous library with a common set of calibration stars (known as the Gaia FGK benchmark stars) that will allow us to assess stellar analysis methods and calibrate spectroscopic surveys.

Methods. High-resolution and signal-to-noise spectra were compiled from different instruments. We developed an automatic process to homogenize the observed data and assess the quality of the resulting library.

Results. We built a high-quality library that will facilitate the assessment of spectral analyses and the calibration of present and future spectroscopic surveys. The automation of the process minimizes the human subjectivity and ensures reproducibility. Additionally, it allows us to quickly adapt the library to specific needs that can arise from future spectroscopic analyses.

Key words. spectroscopy – library – spectral analyses – chemical abundances

1. Introduction

Investigations into how the Milky Way is formed and its evolution are being revolutionized thanks to the many ongoing stellar spectroscopic surveys such as SDSS (York et al. 2000), LAMOST (Zhao et al. 2006), RAVE (Steinmetz et al. 2006), Gaia (Perryman et al. 2001), Gaia-ESO (GES, Gilmore et al. 2012), HERMES/GALAH (Freeman 2010) and APOGEE (Allende Prieto et al. 2008a). Tracing the chemical and dynamical signatures of large samples of stars helps us to distinguish the different Galactic components and thus understand when and how the different Galactic formation scenarios took place. The quantity of spectroscopic data available today requires the development of automatic spectral analysis. Numerous methods have been developed over the past years (e.g., Valenti & Piskunov 1996; Katz et al. 1998; Recio-Blanco et al. 2006; Lee et al. 2008; Koleva et al. 2009; Jofré et al. 2010; Posbic et al. 2012; Mucciarelli et al. 2013; Magrini et al. 2013, to name a few) to assess large datasets, where each of them have different approaches to calibrate and evaluate their results.

Send offprint requests to: S. Blanco-Cuaresma, e-mail: blanco@obs.u-bordeaux1.fr

* Based on NARVAL and HARPS data obtained within the Gaia DPAC (Data Processing and Analysis Consortium) and coordinated by the GBOG (Ground-Based Observations for Gaia) working group, and on data retrieved from the ESO-ADP database.

** The library is available in electronic form at the CDS via anonymous ftp to cdsarc.u-strasbg.fr or via <http://cdsweb.u-strasbg.fr/cgi-bin/qcat?J/A+A/>, and at <http://www.blancocuaresma.com/s/>

However, each survey has its own setup (e.g., spectral range, resolution) and each spectral analysis code has its own particularities (i.e., continuum normalization, atomic line lists). The consequence is that the resulting parameters cannot be directly combined and used for galactic and stellar studies. Thus, spectroscopic calibration with a common reference set of stars is required.

There are several stellar spectral libraries available in the community that are used for calibration in some sense (see, e.g., Munari & Sordo 2005, for a compilation), providing a large sample of good spectra of stars covering a large part of the Hertzsprung-Russel (HR) diagram and metallicities. Examples of them are ELODIE (Prugniel & Soubiran 2001), Indo-US (Valdes et al. 2004), MILES (Sánchez-Blázquez et al. 2006), StarCAT (Ayes 2010), and UVES-POP (Bagnulo et al. 2003). These libraries contain a large number of stars (usually above 1,000) and they differ from each other in terms of resolution and wavelength coverage. They are frequently used for stellar population synthesis models and galactic studies (e.g., Vazdekis et al. 2012; Percival et al. 2009; Zhang et al. 2005, and references therein) and for calibration or validation of methods that determine stellar parameters from stellar spectra (e.g. Allende Prieto et al. 2008b; Koleva et al. 2009; Wu et al. 2011). Nevertheless, the Sun is frequently the only calibration star in common between different methods/surveys and, depending on the survey, its observation is not always possible.

Our motivation for defining the Gaia FGK benchmark stars is to provide a common set of calibration stars beyond the Sun, covering different regions of the HR diagram and spanning a wide range in metallicity. They will be used as pillars for the cali-

bration of the parameters that will be derived for one billion stars by Gaia (Perryman et al. 2001). The defining property of these stars is that we know their radius and bolometric flux, which allows us to estimate their effective temperature and surface gravity *fundamentally*, namely, independent of the spectra. In Heiter et al (in prep, Paper I), we provide the main properties of our sample of the Gaia FGK benchmark stars and describe the determination of temperature and gravity. In this article (Paper II), we introduce the spectral library of the Gaia FGK benchmark stars. In Jofré et al. (2013, Paper III), we analyse our library with the aim to provide a homogeneous scale for the metallicity.

The current sample of Gaia benchmark stars is composed of bright, well-known FGK dwarfs, subgiants, and giants with metallicities between solar and -2.7 dex. We selected stars for which angular diameter and bolometric flux measurements are available or possible. They have accurate parallax measurements, mostly from the HIPPARCOS mission. The sample contains several visual binary stars. In particular, both the A and B components are included for the α Cen and the 61 Cyg systems. The star η Boo is a single-lined spectroscopic binary (Thévenin et al. 2005).

The fastest rotators in the sample are η Boo and HD 49933, with $v \sin i \gtrsim 10 \text{ km s}^{-1}$. The metal-poor dwarf Gmb 1830 has the highest proper motion (4.0 and -5.8 arcsec/yr in right ascension and declination, respectively). Most of the other stars have proper motions less than 1 arcsec/yr.

Our library provides a homogeneous set of high-resolution and high signal-to-noise ratio (S/N) spectra for the 34 benchmark stars. Moreover, the stellar parameters of these benchmark stars were determined consistently and homogeneously, making them perfect for being used as reference. This library of 34 benchmark stars is therefore a powerful tool to cross-calibrate methods and stellar surveys, which is crucial for having a better understanding of the structure and evolution of the Milky Way.

The observed spectra of the benchmark stars were obtained from different telescopes with different instruments and specifications (i.e., resolution and sampling). We developed an automatic process to transform the spectra into one final homogeneous dataset. This allows us to easily generate new versions of the library adapted to the needs of specific surveys (i.e., downgrading the resolution or selecting a different spectral region). Additionally, since reproducibility is one of the main pillars of science, our code will be provided under an open source license to any third party wishes to reproduce the results (Blanco-Cuaresma et al. 2013).

This article is structured as follows. In Sect. 2, we describe the original observed spectra and its sources, while in Sect. 3 we introduce the computer process that was developed to create the library. Section 4 presents the different tests that were performed to validate the correctness of processing and the consistency of the library. In Sect. 5, we describe the resulting library's elements that we provide, and finally, we conclude the paper in Sect. 6

2. Observational data

The original observed spectra come mainly from the archives of three different instruments (NARVAL, HARPS, and UVES). In some cases, observations of the same star were obtained by different telescopes, which gives us the possibility to evaluate instrumental effects (see Table 1 for a general overview).

Table 1. List of the high-resolution spectra available per benchmark star and instrument.

Star	NARVAL	HARPS	UVES	UVES-POP
α Cen A		✓	✓	
α Cen B		✓		
α Cen	✓	✓	✓	
α Tau	✓	✓		
β Ara		✓		
β Gem		✓		
β Hyi		✓	✓	✓
β Vir	✓	✓		
δ Eri	✓	✓	✓	✓
ϵ Eri		✓	✓	✓
ϵ For		✓		
ϵ Vir	✓	✓		
η Boo	✓	✓		
γ Sge	✓			
μ Ara		✓	✓	
μ Cas	✓			
μ Leo	✓			
ψ Phe		✓		
τ Cet	✓	✓		
ξ Hya		✓		
18 Sco	✓	✓		
61 Cyg A	✓			
61 Cyg B	✓			
Arcturus	✓	✓	✓	✓
Gmb 1830	✓			
HD 107328	✓	✓		
HD 122563	✓	✓	✓	✓
HD 140283	✓	✓	✓	✓
HD 220009	✓	✓		
HD 22879	✓	✓		
HD 49933		✓		
HD 84937	✓	✓	✓	✓
Procyon	✓	✓	✓	✓
Sun	✓	✓	✓	

2.1. NARVAL spectra

The NARVAL spectropolarimeter is mounted on the 2m Telescope Bernard Lyot (Aurière 2003) located at Pic du Midi (France). The data from NARVAL were reduced with the LibRESprIT pipeline (Donati et al. 1997). Most of these spectra were taken within a large programme proposed as part of the ‘‘Ground-based observations for Gaia’’ (P.I: C. Soubiran). The benchmark stars observed with this instrument are listed in Table 2, where we indicate the S/N and the radial velocity.

Note that one of the solar spectra was created by co-adding 11 spectra of asteroids with the aim to have higher S/N. The asteroids were observed on different nights, therefore there is no observation date in Table 2. Another solar spectrum corresponding to one single asteroid observation (Metis) with low S/N is included in our sample, which can be used to study S/N effects in spectral analysis.

Table 2. Spectra observed with the NARVAL spectrograph (average resolving power of $\sim 81,000$).

Star	S/N	RV	Date
18 Sco	310 / 393 / 429	11.62 ± 0.05	2012-03-10
61 Cyg A	248 / 375 / 429	-65.84 ± 0.04	2009-10-16
61 Cyg B	290 / 464 / 548	-64.71 ± 0.05	2009-10-13
α Cet	192 / 296 / 367	-26.12 ± 0.04	2009-12-09
α Tau	209 / 319 / 382	54.31 ± 0.04	2009-10-26
Arcturus	283 / 388 / 443	-5.31 ± 0.04	2009-12-11
β Vir	349 / 414 / 437	4.39 ± 0.06	2012-01-09
δ Eri	277 / 356 / 393	-6.27 ± 0.03	2009-10-26
ϵ Vir	309 / 388 / 425	-14.37 ± 0.04	2009-11-27
η Boo	366 / 433 / 452	-6.04 ± 0.12	2009-12-11
γ Sge	301 / 467 / 565	-34.53 ± 0.03	2011-09-30
Gmb 1830	334 / 420 / 458	-98.22 ± 0.07	2012-01-09
HD 107328	278 / 384 / 439	36.41 ± 0.04	2009-11-26
HD 122563	274 / 352 / 398	-26.09 ± 0.18	2009-11-27
HD 140283	265 / 317 / 345	-170.56 ± 0.44	2012-01-09
HD 220009	278 / 384 / 441	40.36 ± 0.04	2009-10-16
HD 22879	256 / 306 / 326	120.37 ± 0.09	2009-11-27
HD 84937	189 / 220 / 231	-14.89 ± 0.51	2012-01-08
μ Cas	220 / 278 / 302	-96.48 ± 0.06	2009-11-26
μ Leo	307 / 415 / 465	13.53 ± 0.03	2011-12-10
Procyon	676 / 790 / 824	-5.75 ± 0.08	2012-03-16
Sun (Metis)	36 / 47 / 52	2.87 ± 0.05	2010-04-25
Sun (co-added)	584 / 723 / 778	5.41 ± 0.05	-
τ Cet	296 / 368 / 399	-16.65 ± 0.05	2009-12-08

Notes. The S/N ratio is reported for three different segments: 480 - 540 / 540 - 610 / 610 - 680 nm. The measured radial velocities are in km/s. The last column corresponds to the observation date.

NARVAL spectra cover a large wavelength range ($\sim 300 - 1100$ nm), with a resolving power¹ that varies for different observation dates and along the wavelength range, typically from 75,000 around 400 nm to 85,000 around 800 nm. However, it is acceptable to initially assume a constant resolving power of $R \approx 81,000$ as we prove in Sect. 4.2.

2.2. HARPS spectra

HARPS is the ESO facility for the measurement of radial velocities with very high accuracy. It is fibre-fed by the Cassegrain focus of the 3.6m telescope in La Silla (Mayor et al. 2003). The spectra were reduced by the HARPS Data Reduction Software (version 3.1). Most of the data for benchmark stars were obtained within the programme for critical tests on stellar atmosphere models within the Gaia-SAM collaboration (P.I: U. Heiter). The remaining HARPS data were taken from the public archives.

The list of HARPS spectra can be found in Table 3. The solar spectra correspond to two observations of asteroids (Ceres and Vesta) and one observation of one of Jupiter's moons (Ganymede). We could obtain them directly from the public archive thanks to Molaro & Monai (2012), who presented a detailed analysis of absorption lines of the those spectra. Additionally, we co-added those spectra to have a solar spectrum with higher S/N.

¹ The terms "resolving power" and "resolution" refer to the relation $R = \frac{\lambda}{\Delta\lambda}$, although we prefer to use the former when talking about instrumental capabilities and the latter for already observed spectra

Table 3. Spectra observed with the HARPS instrument (average resolving power of $\sim 115,000$).

Star	S/N	RV	Δ RV	Date
18 Sco	146 / 168 / 173	11.82 ± 0.04	-0.02	2009-05-20
α Cen A	381 / 442 / 487	-22.6 ± 0.04	-0.02	2005-04-08
α Cen A	433 / 495 / 540	-22.6 ± 0.04	-0.02	2005-04-19
α Cen B	393 / 467 / 507	-21.86 ± 0.03	-0.05	2005-04-08
Arcturus	368 / 470 / 554	-5.19 ± 0.03	-0.01	2004-07-08
β Hyi	381 / 424 / 465	23.16 ± 0.05	0.01	2005-11-13
β Vir	272 / 313 / 329	4.55 ± 0.05	0.03	2009-04-10
δ Eri	436 / 521 / 576	-6.21 ± 0.03	-0.04	2005-10-23
ϵ Eri	383 / 474 / 537	16.4 ± 0.04	-0.05	2005-12-28
HD 49933	293 / 323 / 329	-12.06 ± 0.19	0.06	2011-01-05
μ Ara	207 / 250 / 275	-9.35 ± 0.04	-0.02	2004-06-08
Sun-1 (Ceres)	227 / 253 / 267	3.99 ± 0.04	0.07	2006-07-16
Sun-2 (Gan.)	312 / 362 / 389	6.02 ± 0.04	-0.02	2007-04-13
Sun-3 (Vesta)	174 / 194 / 201	3.77 ± 0.04	0.0	2009-12-25
Sun (co-added)	421 / 483 / 514	3.97 ± 0.04	-	-
τ Cet	219 / 260 / 282	-16.57 ± 0.04	-0.04	2008-09-09
α Cet	165 / 228 / 284	-25.66 ± 0.04	-0.16	2007-10-22
α Tau	47 / 69 / 86	54.21 ± 0.03	-0.06	2007-10-22
β Ara	285 / 408 / 488	0.22 ± 0.04	0.25	2007-09-29
β Gem	287 / 359 / 416	3.42 ± 0.03	-0.04	2007-11-06
ϵ For	281 / 330 / 358	40.8 ± 0.04	-0.01	2007-10-22
ϵ Vir	319 / 386 / 421	-14.28 ± 0.03	-0.02	2008-02-24
η Boo	358 / 410 / 439	-2.23 ± 0.12	0.06	2008-02-24
HD 107328	343 / 452 / 524	36.66 ± 0.03	-0.02	2008-02-24
HD 122563	353 / 430 / 492	-26.24 ± 0.17	0.07	2008-02-24
HD 140283	441 / 497 / 535	-170.46 ± 0.42	0.05	2008-02-24
HD 220009	262 / 342 / 398	40.18 ± 0.04	0.01	2007-10-22
HD 22879	296 / 322 / 336	120.38 ± 0.08	-0.03	2007-10-22
HD 84937	444 / 484 / 513	-14.76 ± 0.49	0.24	2007-12-03
ξ Hya	318 / 386 / 422	-4.53 ± 0.04	-0.01	2008-02-24
Procyon	352 / 373 / 377	-3.11 ± 0.08	0.0	2007-11-06
ψ Phe	274 / 352 / 460	3.07 ± 0.06	-0.31	2007-09-30

Notes. The S/N ratio is reported for three different segments: 480 - 540 / 540 - 610 / 610 - 680 nm. The measured radial velocities are in km/s and Δ RV is the difference from the reported velocity by HARPS pipeline. The last column corresponds to the observation date.

The spectra for the stars HD84937 and HD140283 are the result of the co-addition of four and two individual observed spectra, respectively. The reason for combining these spectra is to increase the S/N. The spectra of each star were taken on the same night, with the date indicated in Table 3.

The spectral range covered is 378 – 691 nm, but as the detector consists of a mosaic of two CCDs, one spectral order (from 530 nm to 533 nm) is lost in the gap between the two chips.

2.3. UVES spectra

The UVES spectrograph is hosted by unit telescope 2 of ESO's VLT (Dekker et al. 2000). We took the spectra of benchmark stars available the Advanced Data Products collection of the ESO Science Archive Facility² (reduced by the standard UVES pipeline version 3.2, Ballester et al. 2000) by selecting only the most convenient³ spectrum for each star based on visual inspection.

² http://archive.eso.org/eso/eso_archive_adp.html

³ Those spectra with high S/N and smooth continuum, given that sometimes the merging of the orders did not produce a smooth spectrum along the wavelength range

Table 4. Spectra observed with the UVES instrument.

Star	S/N	RV	R	Date
α Cen A	287 / 328 / 324	-23.13 ± 0.04	90000 85000	2000-04-11
α Cet	157 / 209 / 227	-25.53 ± 0.04	115000 90000	2003-08-11
Arcturus	213 / 291 / 306	-5.18 ± 0.03	115000 95000	2004-08-03
β Hyi	407 / 447 / 411	22.96 ± 0.05	85000 78000	2001-07-27
δ Eri	176 / 208 / 217	-5.87 ± 0.03	85000 75000	2001-11-29
ϵ Eri	204 / 231 / 222	15.99 ± 0.04	115000 90000	2001-10-02
HD 122563	288 / 326 / 327	-26.66 ± 0.17	82000 72000	2002-02-19
HD 140283	279 / 305 / 298	-170.79 ± 0.41	85000 78000	2001-07-09
HD 84937	215 / 229 / 228	-15.19 ± 0.48	80000 72000	2002-11-28
μ Ara	292 / 327 / 309	-9.25 ± 0.04	115000 95000	2003-09-05
Procyon	349 / 379 / 356	-2.35 ± 0.08	82000 75000	2002-10-08
Sun (Vesta)	337 / 383 / 418	-5.52 ± 0.04	78000 78000	2000-10-18

Notes. The S/N ratio is reported for three different segments: 480 - 540 / 540 - 610 / 610 - 680 nm. The measured radial velocities are in km/s. The reported resolving power correspond to the lower and upper parts of each spectrum. The last column corresponds to the observation date.

Table 5. Spectra observed with the UVES instrument and processed by the UVES-POP pipeline (average resolving power of 80,000).

Star	S/N	RV	Date
Arcturus	1123 / 1312 / 1235	-5.48 ± 0.03	2003-02-16
β Hyi	596 / 690 / 717	22.99 ± 0.06	2001-07-25
δ Eri	421 / 547 / 606	-5.94 ± 0.03	2001-11-28
ϵ Eri	1468 / 1625 / 1808	16.09 ± 0.04	2002-10-11
HD 122563	846 / 934 / 624	-26.73 ± 0.18	2002-08-18
HD 140283	807 / 901 / 864	-170.75 ± 0.43	2001-07-08
HD 84937	511 / 537 / 567	-15.13 ± 0.48	2002-11-28
Procyon	1297 / 1449 / 948	-2.25 ± 0.08	2002-10-07

Notes. The S/N ratio is reported for three different segments: 480 - 540 / 540 - 610 / 610 - 680 nm. The measured radial velocities are in km/s. The last column corresponds to the observation date.

The setup used for each observation (CD#3, centered around 580 nm) provides a spectrum with two different parts which approximately cover the ranges from 476 to 580 nm (lower part) and from 582 to 683 nm (upper part). The resolution of each spectrum and lower/upper parts might be different depending on the slit width used during the observation. There is a relation between the slit width (or the seeing if it is considerable smaller than the slit width) and the resolution, which depends on the date of observation⁴. We went through those relations for each spectrum and estimated its resolution which can be found in Table 4.

2.4. UVES-POP spectra

The UVES Paranal Observatory Project UVES-POP library (Bagnulo et al. 2003, processed with data reduction tools specifically developed for that project) contains stellar spectra along the complete UVES wavelength range (300-1000 nm with two gaps around 580 nm and 860 nm). The benchmark stars that are included in this library are listed in Table 5.

⁴ http://www.eso.org/observing/dfo/quality/UVES/reports/HEALTH/\trend_report_ECH_RESOLUTION_DHC_HC.html

2.5. Atlas spectra

We included the already normalized atlas spectra from Hinkle et al. (2000) for the Sun and Arcturus. The observations were made with the Coude Feed Telescope on Kitt Peak with the spectrograph in the Echelle mode, reaching a resolving power of 150,000 and a high S/N. The authors of that work also removed the telluric lines from the provided spectra.

The inclusion of this observations in the library is only for normalization validation purposes (see Sect. 4.1); they were not treated by the same homogeneous normalization process as the other spectra.

3. Data handling and processing

An automatic computational process was developed to transform the observed spectra presented in Sect. 2 into a homogeneous library of the benchmark stars. Since the wavelength range varies from one set of observations to another, we chose to limit the current library to the range between 480 and 680 nm, where all the spectra provide their best S/N. Additionally, the range matches the interests of the Gaia-ESO Survey (GES, Gilmore et al. 2012) given their UVES setup on the ESO-VLT telescope.

In this section, we describe how the data are treated to determine and correct the radial velocity of the star, fit the continuum and normalize, convolve the spectra to a common desired resolution, and re-sample the spectra to finally obtain a homogeneous library (see Fig. 1 for a general overview).

3.1. Cleaning and cosmic rays removal

The spectra obtained by different instruments have different conventions to indicate errors in the observation. For instance, bad pixels can be marked with negative fluxes. These values should not be considered as good data, therefore we automatically ignore them.

On the other hand, spectra may contain residuals from cosmic rays which can affect the normalization process and future analyses. We implemented an algorithm that detects them automatically using a median filter to smooth out single-measurement deviations. The process is as follows:

1. Re-sample the spectrum to have a homogeneous sampling of 0.001 nm steps (small enough to respect the original resolution).
2. Obtain a smoothed spectrum by applying a median filter with a window of 15 points, which equals to 0.015 nm.
3. Re-sample the smoothed spectrum to the original wavelength grid again.
4. Subtract the smoothed spectrum from the original one.
5. Mark all the points with differences higher than 0.01 (1% of total flux) which are located above the continuum as cosmic rays (determined by a preliminary execution of the steps described in Sect. 3.5).

Cosmic rays may also appear under the continuum, but if we attempt to remove them, we might also affect the upper parts of sharply blended lines. Therefore, we preferred to limit ourselves to cosmic rays above the continuum.

3.2. Co-addition

As specified in Sect. 2.2, several spectra observed by HARPS were co-added for the stars HD140283 and HD84937. Addition-

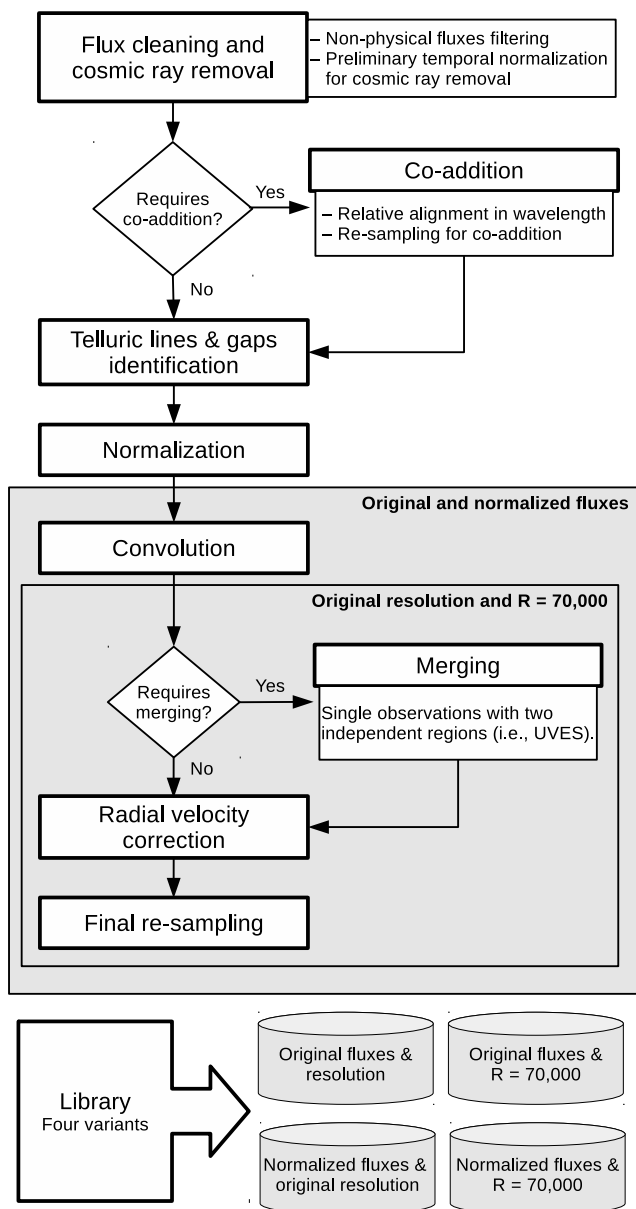


Fig. 1. Flowchart of the automatic computational process developed to build the library.

ally, three solar spectra observed by HARPS and 11 asteroids observed by NARVAL were co-added into two single spectra (one per instrument).

For each co-addition, we selected one spectrum as reference, we removed those regions that are potentially affected by telluric lines (see Sect. 3.3) and we executed a cross-correlation process (see Sect. 3.8.2) against the other spectra of the same star. Finally, we aligned all the spectra (zero differential velocity), re-sampled them (see Sect. 3.9), and summed up their fluxes.

3.3. Telluric lines

Telluric lines from Earth’s atmosphere contaminate ground-observed spectra and might affect stellar analyses. We identified automatically those potentially affected regions which allows the users to easily ignore or remove them.

In this process, a synthetic spectrum from TAPAS (Bertaux et al. 2013) was used. TAPAS is an on-line service that provides simulated atmospheric transmission spectra for specific observing conditions.

We do not need to recover the exact telluric spectrum for the day and place of observation since our goal is not to correct them but to identify the potentially affected regions. Therefore, we obtained a synthetic spectrum as if all the observations were done at ESO observatory (La Silla, Chile) pointing to the zenith (angle of zero degrees).

Once the non-convolved synthetic spectrum was obtained and normalized (as described in Sect. 3.5), an automatic process for absorption line detection was applied. The process performs the following steps:

1. Search local minimum (representing absorption peaks) and maximum points (corresponding to the limits of the absorption line).
2. Discard lines found that are false positive or noise by ignoring:
 - (a) peaks that have a smaller depth than its nearby maximums (false positives),
 - (b) peaks too close (2 or less bins away) to the next and previous maximums (noise);
3. Discard those line candidates that do not have a minimum depth (1.0% of depth with respect to the continuum).
4. Fit a Gaussian model to the line candidates.
5. Discard lines with bad fits.

The process provides us with the position of the telluric lines peaks and the full-width at half-maximum (FWHM) of the fitted Gaussian. In order to delimit where the lines start and end, we searched for local maximums $4 \times \text{FWHM}$ around each telluric line’s peak or we directly used $2 \times \text{FWHM}$ if no local maximum was found.

The resulting telluric line list was used as a mask for locating the telluric lines in each observed spectra by using cross-correlation (as the one described in Sect. 3.8.2). The identified regions affected by telluric lines were ignored in the normalization process (Sect. 3.5).

3.4. Gaps

Depending on the instrument, some spectra contain gaps (regions without fluxes or all fluxes set to zero). We identified them automatically to be able to easily ignore those regions.

3.5. Normalization

The spectra were normalized automatically, reducing biases and inhomogeneities due to subjective criteria. For each observed star, the process uses a synthetic spectrum generated with the MARCS model atmospheres (Gustafsson et al. 2008), an atomic line list from VALD (Kupka et al. 2011), the SPECTRUM code (Gray & Corbally 1994) and the atmospheric parameters listed in Table 6. The fitting algorithm is as follows:

1. Ignore all the fluxes that have a value below 0.98 in their respective synthetic spectra (computed with the reference atmospheric parameters). This way, we reduce the effect of strong lines in the normalization process.
2. Ignore gaps and regions affected by telluric lines.
3. Reduce the noise effects by applying a median filter with a window of 0.01nm (window sizes were selected after several validation and optimization tests).

Table 6. Parameters used for the spectral synthesis in the normalization process.

Star	Teff	log(g)	[M/H]	Vmic	Vmac	v sin(i)
ψ Phe	3472	0.51	-1.23	1.54	6.26	3.00
α Cet	3796	0.68	-0.45	1.36	5.68	3.00
γ Sge	3807	1.05	-0.16	1.43	5.01	6.00
α Tau	3927	1.11	-0.37	1.36	5.23	5.00
61 Cyg B	4044	4.67	-0.38	0.85	5.00	1.70
β Ara	4173	1.04	-0.05	1.24	5.09	5.40
HD 220009	4275	1.47	-0.75	1.23	5.39	1.00
Arcturus	4286	1.64	-0.53	1.25	5.05	3.80
61 Cyg A	4374	4.63	-0.33	0.86	4.19	0.00
μ Leo	4474	2.51	0.26	1.28	3.63	5.10
HD 107328	4496	2.09	-0.34	1.23	4.60	1.90
HD 122563	4587	1.61	-2.74	1.13	6.13	5.00
Gmb 1830	4827	4.60	-1.46	0.82	3.49	0.50
β Gem	4858	2.90	0.12	1.22	3.68	2.00
δ Eri	4954	3.75	0.06	1.00	3.60	0.70
ϵ Vir	4983	2.77	0.13	1.23	3.78	2.00
ξ Hya	5044	2.87	0.14	1.23	3.72	2.40
ϵ Eri	5076	4.60	-0.10	0.88	3.22	2.40
ϵ For	5123	3.52	-0.62	1.02	4.05	4.20
α Cen B	5231	4.53	0.22	0.93	2.79	1.00
μ Cas	5308	4.41	-0.82	0.91	3.85	0.00
τ Cet	5414	4.49	-0.50	0.94	3.70	0.40
HD 140283	5514	3.57	-2.43	1.05	5.18	5.00
Sun	5777	4.44	0.02	1.07	4.19	1.60
α Cen A	5792	4.30	0.24	1.11	4.01	1.90
18 Sco	5810	4.44	0.01	1.08	4.34	2.20
HD 22879	5868	4.27	-0.88	1.09	5.45	4.40
β Hyi	5873	3.98	-0.07	1.16	4.82	3.30
μ Ara	5902	4.30	0.33	1.15	4.40	2.20
β Vir	6083	4.10	0.21	1.24	5.62	2.00
η Boo	6099	3.80	0.30	1.30	5.74	12.70
HD 84937	6356	4.15	-2.09	1.29	9.24	5.20
Procyon	6554	3.99	-0.04	1.48	9.71	2.80
HD 49933	6635	4.20	-0.46	1.48	10.87	10.00

Notes. The effective temperature (K) and surface gravity (dex) were obtained from Paper I, the metallicity corresponds to the Fe I LTE abundances (dex) from Paper III (SPECTRUM code assumes Local Thermodynamic Equilibrium, LTE), the micro/macroturbulence (km/s) is derived from an empirical relation calibrated by the Gaia ESO Survey working groups (M. Bergemann and V. Hill, private communication) and the rotation (km/s) found in the literature (see Papers I/III).

4. Apply a maximum filter with a window of 1.0nm to select those fluxes that have more probabilities belonging to the continuum.
5. Fit second degree splines every 1.0nm to the filtered points and divide the original observed spectrum by the fitted model.

After several tests, we found this was the most robust strategy to homogeneously normalize the library's spectra.

3.6. Resolution degradation

The resulting final library was homogenized to the highest minimum resolving power, which corresponds to 70,000. The process convolves the spectra by performing the following steps for each flux value:

1. Define a window with size $FWHM_\lambda$ which depends on the original and final desired resolution:

$$FWHM_\lambda = \sqrt{\left(\frac{\lambda}{R_{\text{final}}}\right)^2 - \left(\frac{\lambda}{R_{\text{initial}}}\right)^2}. \quad (1)$$

2. Build a Gaussian profile $g(\lambda_x)$ using the sigma corresponding to $FWHM_\lambda$ and the wavelength values of a spectral window around the wavelength λ that it is going to be convolved:

$$g(\lambda_x) = \frac{1}{\sqrt{2\pi\sigma_\lambda^2}} e^{-\frac{(\lambda_x-\lambda)^2}{2\sigma_\lambda^2}}, \quad (2)$$

$$\text{where } \sigma_\lambda = \frac{FWHM_\lambda}{2\sqrt{2\log 2}}.$$

3. Normalize the Gaussian profile and multiply it by the original fluxes in the spectral window. The sum of that operation will be the new convolved value for the wavelength λ :

$$\text{flux}(\lambda) = \sum_{\text{window}}^x \text{flux}(\lambda_x) \left(\frac{g(\lambda_x)}{\sum_{\text{window}}^x g(\lambda_x)} \right). \quad (3)$$

3.7. Merge

The spectra from the UVES instrument were observed with a setup that provides a separate lower and upper spectral part (see Sect. 2.3). In these cases, we performed the cleaning, normalization and convolution separately and, afterwards, the resulting spectra were merged.

3.8. Radial velocity

3.8.1. Zero point template

As a zero point we could use, for instance, the solar HARPS spectrum since this instrument provides high precision radial velocity measurements. We preferred to use the co-added solar NARVAL spectrum because it does not contain any gap, however, in order to transform the NARVAL solar spectrum into a reliable zero point template, we removed the regions affected by telluric lines and we cross-correlated it with a solar HARPS spectrum, which was corrected by using the radial velocity reported by HARPS pipeline. Finally, we corrected the NARVAL spectrum with the relative velocity shift found.

3.8.2. Cross-correlation

The first stage in the radial velocity determination process is the generation of the velocity profile by the cross-match correlation algorithm (Pepe et al. 2002), which sums the spectrum's fluxes multiplied by a mask/template function 'p':

$$C(v) = \sum_{\lambda} p(\lambda, v) \cdot \text{flux}(\lambda), \quad (4)$$

where v is the velocity.

1. Create a wavelength grid uniformly spaced in terms of velocity. This means that an increment in position ($x \rightarrow x+1$) supposes a constant velocity increment (velocity step) but a variable wavelength increment. The following formula is used

for determining the wavelength ranges (relativistic Doppler effect):

$$\lambda_{x+1} = \lambda_x + \lambda_x \left(1 - \sqrt{\frac{1 - \frac{v}{c}}{1 + \frac{v}{c}}} \right), \quad (5)$$

where c is the speed of light in vacuum and λ the original wavelengths.

2. Calculate the cross-correlation function (Baranne et al. 1996; Allende Prieto 2007) between the spectrum and the specified template by shifting the template from limits (see below).

Once the velocity profile was constructed from the cross-correlation process, the mean velocity is calculated by fitting a second order polynomial near the peak. Additionally, a Gaussian model is fitted (with fixed mean velocity) to determine other complementary parameters such as the FWHM.

The whole process is repeated two times: Firstly a general estimation is obtained by using a velocity step of 5.0 km/s (1.0 km/s if we are cross-correlating with a telluric line mask) with lower and upper limits of ± 200 km/s; Secondly, a more precise value is determined by using a step of 0.25 km/s with lower and upper limits of $\pm 4 \times \text{FWHM}$ around the first velocity estimation.

The error in the radial velocity determination is calculated by following Zucker (2003):

$$\sigma_v^2 = - \left[N \frac{C''(v)}{C(v)} \frac{C^2(v)}{1 - C^2(v)} \right]^{-1}, \quad (6)$$

where N is the number of bins in the spectrum, C is the cross-correlation function, and C'' is its second derivative.

Finally, the correction is performed by applying the following formula:

$$\lambda_{corrected} = \lambda \sqrt{\frac{1 - \frac{v}{c}}{1 + \frac{v}{c}}}. \quad (7)$$

3.9. Re-sampling

The final step in the homogenization process is to sample all the spectra by establishing a constant increment in wavelength (0.001 nm) from 480 to 680 nm. To do so, we implemented a Bessel's Central-Difference interpolation similar to that used in TGMET (Katz et al. 1998).

A quadratic Bessel's interpolation formula was employed. It makes use of two points before and two points after the value to be interpolated (except where there are not enough, such as at the beginning and end of the spectrum, where a linear interpolation is performed). The formula is as follows:

$$f(\lambda) = f(\lambda_0) + p(f(\lambda_1) - f(\lambda_0)) + \left[\frac{p(p-1)}{4} \right] (f(\lambda_2) - f(\lambda_1) - f(\lambda_0) + f(\lambda_{-1})), \quad (8)$$

where $p = \frac{\lambda - \lambda_0}{\lambda_1 - \lambda_0}$, $f(\lambda)$ is the flux, λ is the target wavelength, and $\lambda_{-1} < \lambda_0 < \lambda < \lambda_1 < \lambda_2$. The zero and first order terms correspond to a linear interpolation, while the second order term is a correction factor to that linear interpolation.

3.10. Errors

All the observed spectra have individual errors associated with each measured flux except the atlas spectra. For the latter, we estimated the errors dividing the fluxes by the S/N, which was obtained by calculating the ratio between the mean flux and the standard deviation for groups of ten measurements around each wavelength point and selecting the mean value.

For the operations that implied flux modification (e.g., convolution, continuum normalization), the errors were taken into account and appropriately propagated.

4. Validation

The resulting library was evaluated to guarantee that the data were properly treated and that the spectra present a high level of quality.

4.1. Normalization

The normalization process should produce similar spectra for the same stars independent of the instrument used for the observation. To validate that statement and therefore the internal coherence, we compared spectra from different instruments by calculating their root mean square (RMS) difference in flux as:

$$\text{RMS} = \sqrt{\frac{\sum (\text{flux}_{\text{reference}} - \text{flux})^2}{\text{num_fluxes}}}, \quad (9)$$

where $\text{flux}_{\text{reference}}$ is the flux from a given spectrum (i.e., the first in the treatment chain).

The test was performed using the whole wavelength range and three individual regions: H- α (653 - 660 nm), H- β (483 - 489 nm), and Mg triplet (515 - 520 nm). Regions affected by telluric lines or gaps were not considered in the comparison.

No general trends as a function of wavelength or systematic effects were found even in difficult regions with strong lines such as H- α and the Mg triplet (see Fig. 2). The mean relative difference⁵ is 0.001 ± 0.002 (0.1%) and the average RMS is 0.009 ± 0.004 , which as expected depends on the type of the star (see Table 7) since colder stars have more absorption lines and the continuum fitting process becomes more difficult.

Additionally, we compared our normalized spectra with the atlas spectra (Sun and Arcturus), which were normalized by an independent external procedure. The mean relative difference is -0.001 ± 0.002 (-0.1%) for the Sun and $-0.003\% \pm 0.002\%$ (-0.3%) for Arcturus. The average RMS is smaller than 0.02 (see Table 8) and no systematic effects were found. The normalization in strong line regions is also consistent (see Fig. 2).

4.2. Resolution

In order to assess the quality of a spectrum, it is important to validate that the assumed initial resolving power is correct and that the convolution process works correctly.

We assumed that the final resulting library has a resolution of 70,000, which corresponds to a FWHM of 4.28 km/s ($\text{FWHM} = \frac{c}{R}$). By using only the regions affected by the telluric lines, we cross-correlated the original and convolved normalized spectrum with the telluric mask and we obtained the FWHM in both cases (FWHM_1 and FWHM_2 respectively). Therefore, we

⁵ The mean relative difference is defined by $\Delta \text{flux} = \frac{\text{flux}_{\text{reference}} - \text{flux}}{\text{flux}_{\text{reference}}}$

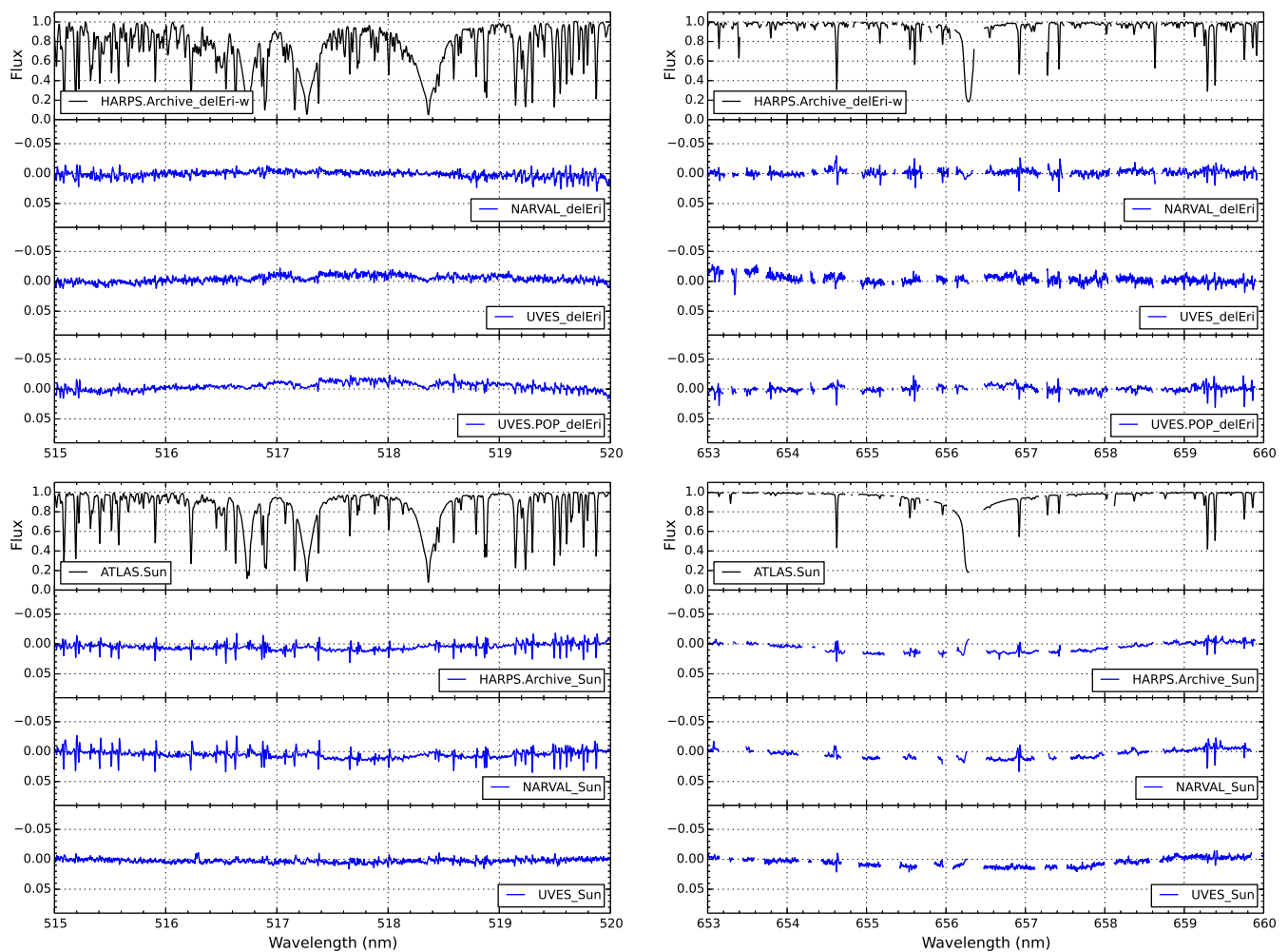


Fig. 2. Normalization comparison for δ Eri (upper part) and the Sun (lower part). The spectra of reference are in black and the flux differences with the remaining observation are in blue. The regions compared correspond to the magnesium triplet (left) and H- α (right). Regions affected by tellurics were removed.

can quantify how much the FWHM was changed as a result of the convolution process and validate that the difference is consistent with the expected initial resolution, that is,

$$\Delta FWHM_{\text{cross}} = (4.28 + (FWHM_1 - FWHM_2)) - (c/R_{\text{initial}}), \quad (10)$$

where c is the speed of light and R_{initial} the expected initial resolution (see Tables 2, 3, 4, and 5), should be close to zero.

The results⁶ presented in Table 9 are in general agreement with the expected original resolving power. UVES spectra show the biggest dispersion in measured original resolving power, which is natural since not all the original spectra share the exact same resolving power (it can even vary between the lower and higher parts of the spectrum).

We recall that NARVAL resolving power is not constant along the entire wavelength range. To show that this is not problematic, we measured the individual FWHM of a group of stellar lines (see Sect. 4.4) for each spectra. For those stars with

⁶ Atlas spectra were not considered since the telluric lines are not present in the original spectra.

more than one spectrum, we calculated the relative difference in FWHM for the lines in common (see Table 10):

$$\Delta FWHM = \frac{FWHM_{\text{other}} - FWHM_{\text{HARPS}}}{FWHM_{\text{HARPS}}}. \quad (11)$$

The relative difference in FWHM for a spectrum observed by HARPS and NARVAL compared to the same spectrum observed by HARPS and UVES is not significant as we show in Fig. 3. The variable resolving power of NARVAL is small enough to be neglected and it does not have a relevant impact in spectroscopic analyses, such as the one performed in Paper III.

4.3. Radial velocity

The HARPS pipeline provides high precision radial velocity measurements for each observed spectrum. We used those measurements to test our radial velocity determination method and we obtained a zero mean difference with a standard deviation of 0.08. The individual differences can be found in Table 3.

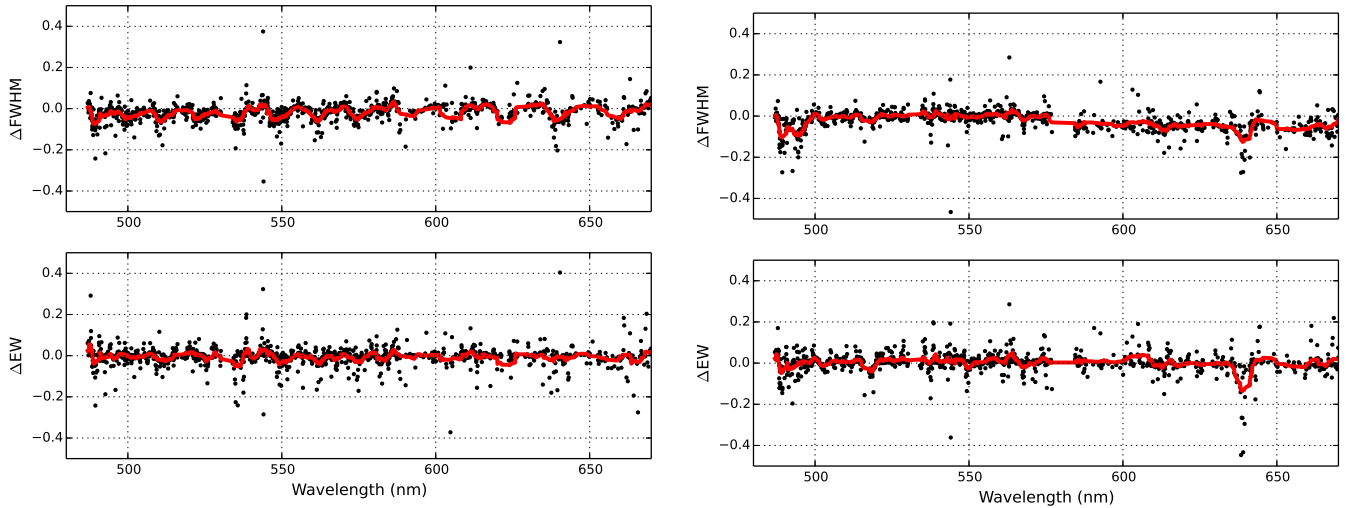


Fig. 3. Relative difference in FWHM (upper part) and equivalent widths (lower part) for the δ Eri spectrum, with the moving average overplotted (red) for visual guidance. The numeric details of the HARPS against NARVAL (left plot) and HARPS against UVES-POP (right plot) comparisons can be found in Table 10.

Table 7. Average RMS difference in flux for the normalized spectra of the same star but observed by different instruments.

Star	All	H- α	H- β	MgTriplet
α Cen A	0.012	0.009	0.008	0.004
α Cen	0.021	0.015	0.026	0.018
α Tau	0.014	0.010	0.015	0.013
β Hyi	0.009	0.009	0.008	0.003
β Vir	0.007	0.007	0.006	0.005
δ Eri	0.008	0.006	0.010	0.007
ϵ Eri	0.015	0.015	0.008	0.007
ϵ Vir	0.006	0.005	0.006	0.006
η Boo	0.005	0.005	0.005	0.004
μ Ara	0.012	0.014	0.011	0.008
τ Cet	0.007	0.008	0.007	0.005
18 Sco	0.007	0.009	0.007	0.007
Arcturus	0.010	0.010	0.012	0.015
HD 107328	0.006	0.008	0.008	0.009
HD 122563	0.008	0.007	0.007	0.004
HD 140283	0.009	0.006	0.006	0.004
HD 220009	0.006	0.005	0.007	0.007
HD 22879	0.007	0.006	0.007	0.005
HD 84937	0.007	0.005	0.009	0.005
Procyon	0.013	0.008	0.008	0.005
Sun	0.008	0.004	0.008	0.005
Mean	0.009	0.008	0.009	0.007
StdDev	0.004	0.003	0.004	0.004

Notes. Apart from the whole wavelength range (All), three individual regions are also reported: H- α (653 - 660 nm), H- β (483 - 489 nm), and Mg triplet (515 - 520 nm).

4.4. Equivalent widths

Different observations of the same Benchmark Star with the same resolution should have the same equivalent widths (EW). Thus, measuring and comparing EW provides us a different perspective to validate the normalization and convolution processes.

In that sense, we used the lines from Ramírez & Allende Prieto (2011) for the Sun and Arcturus, which are good repre-

Table 8. Mean RMS differences in flux for atlas spectra and our normalized spectra observed by different instruments.

Star	All	H- α	H- β	MgTriplet
Arcturus	0.015	0.023	0.022	0.018
Sun	0.009	0.009	0.018	0.007

Table 9. Mean difference between expected and measured FWHM in km/s (see Eq. 10) and mean estimated original resolving power with their corresponding standard deviation.

Instrument	$\Delta\text{FWHM}_{\text{cross}}$	Estimated R_{initial}
	$\mu \pm \sigma$	$\mu \pm \sigma$
HARPS	-0.07 ± 0.21	118825 ± 9655
NARVAL	0.10 ± 0.13	79050 ± 2999
UVES	0.19 ± 0.14	83200 ± 10397
UVES.POP	-0.01 ± 0.15	80932 ± 3942

Table 10. Difference in FWHM and equivalent widths between HARPS observations and the other instruments.

Star	Instrument	ΔFWHM	ΔEW
		$\mu \pm \sigma$	$\mu \pm \sigma$
Sun	NARVAL	-0.08 ± 0.05	-0.00 ± 0.03
Sun	UVES	-0.05 ± 0.04	-0.02 ± 0.06
Arcturus	NARVAL	-0.06 ± 0.03	0.02 ± 0.02
Arcturus	UVES	0.00 ± 0.03	0.03 ± 0.03
Arcturus	UVES.POP	-0.05 ± 0.03	0.02 ± 0.03
18 Sco	NARVAL	-0.00 ± 0.07	0.02 ± 0.07
δ Eri	NARVAL	-0.02 ± 0.05	-0.01 ± 0.05
δ Eri	UVES	0.01 ± 0.05	0.00 ± 0.06
δ Eri	UVES.POP	-0.02 ± 0.05	0.00 ± 0.05
η Boo	NARVAL	0.00 ± 0.04	0.00 ± 0.05
HD 220009	NARVAL	-0.02 ± 0.05	-0.01 ± 0.06
Procyon	NARVAL	-0.01 ± 0.05	-0.00 ± 0.06
Procyon	UVES	0.03 ± 0.07	0.01 ± 0.09
Procyon	UVES.POP	0.02 ± 0.05	0.02 ± 0.11
Mean		-0.02 ± 0.03	0.01 ± 0.01

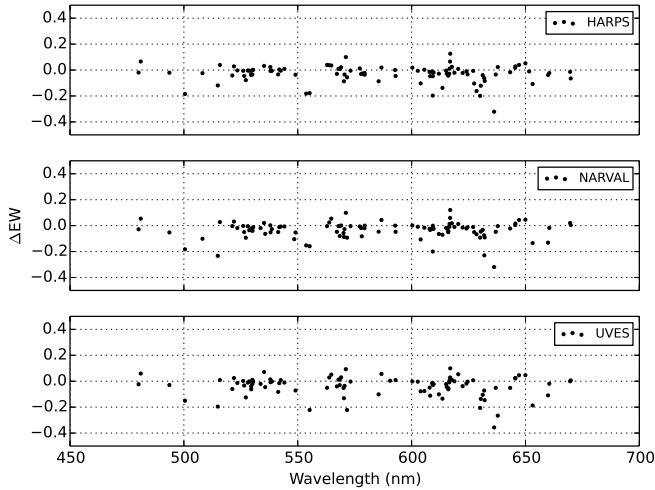


Fig. 4. Relative differences in the equivalent width measured for the Sun by [Ramírez & Allende Prieto \(2011\)](#).

representatives for the dwarf and giant stellar types. The authors derived the EWs from high resolution spectra ($R > 300,000$ ⁷ for the Sun, [Kurucz et al. \(1984\)](#), $R \sim 100,000$ for Arcturus ([Hinkle & Wallace 2005](#))), therefore we used the original non-convolved observations of the Benchmark Stars for the comparison.

The analysis was complemented with the inclusion of lines measured by [Luck & Heiter \(2006\)](#) and [Luck & Heiter \(2007\)](#) for 11 additional stars (seven dwarfs, four giants). In this case, the authors measured the EWs from spectra with a resolving power of 60,000. In consequence, we downgraded the resolution of the corresponding stars to match the same value and thereby equalize the conditions (i.e., same degree of blends).

Our EWs are determined by fitting a Gaussian profile in each absorption line and integrating its area. In the process, we discarded those lines that do not present a good fit (i.e., $RMS > 0.05$). The relative EW difference is calculated as:

$$\Delta EW = \frac{EW_{external} - EW}{EW}. \quad (12)$$

4.4.1. External consistency

We obtained a high level of consistency with the independently measured EWs (see Fig. 4 and Fig. 6), the mean relative EW difference is around -0.03 ± 0.07 for the Sun and -0.03 ± 0.12 for Arcturus. The dispersion is logically higher for the latter since the continuum in giants is less trivial to fit.

The visual inspection of lines with higher relative EW differences (see Fig. 5 and Fig. 7) shows that our fit is consistent. The cause of the differences seems to be related to the continuum placement, which is specially amplified for weak absorption lines.

The additional stars present the same high level of agreement with a mean relative difference of -0.01 ± 0.04 (1%), all the detailed results can be found in Table 11.

⁷ <http://kurucz.harvard.edu/sun/fluxatlas/fluxatlastext.tab>

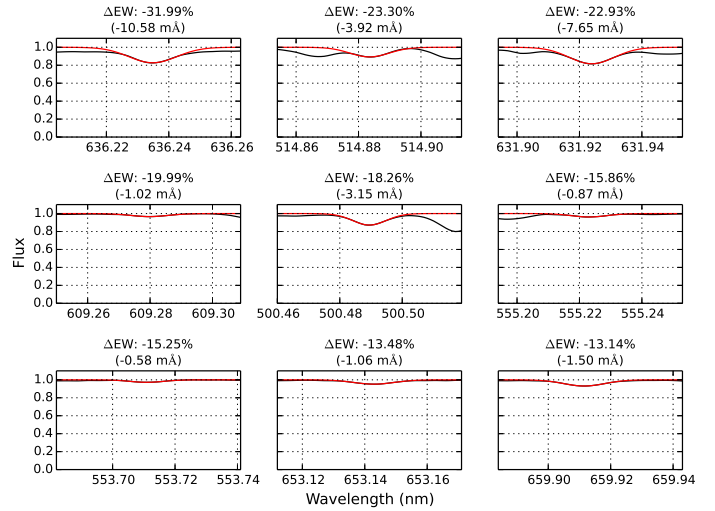


Fig. 5. Normalized fluxes (black) and fitted Gaussians (red) for the lines with the highest relative difference in EW compared to [Ramírez & Allende Prieto \(2011\)](#). The fluxes correspond to the co-added spectra of the Sun observed by NARVAL.

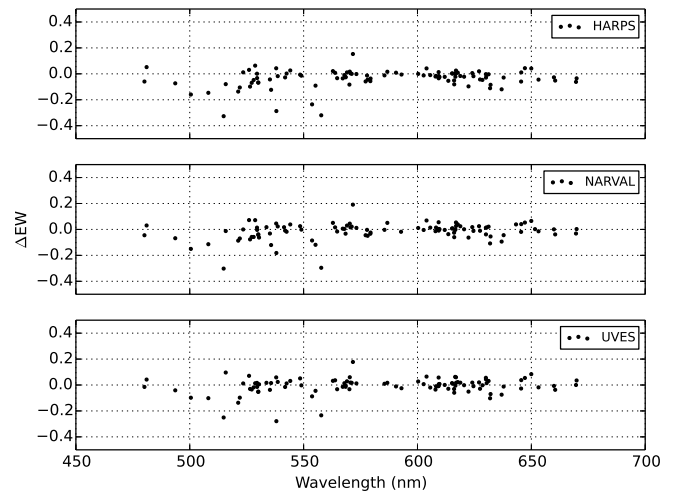


Fig. 6. Relative differences in the equivalent width measured for Arcturus by [Ramírez & Allende Prieto \(2011\)](#).

4.4.2. Internal consistency

We compared the measured EWs from those stars observed by different instruments. The level of internal consistency is very high (see Fig. 3) and the mean relative EW difference is 0.01 ± 0.01 (1%) as shown in Table 10. We estimated that abundance analysis based on EW methods show a very small variation of the order of ± 0.007 dex in metallicity when EWs are changed by 1% (based on the analysis of a solar spectrum).

5. Resulting library

The latest version of the library can be downloaded from <http://www.blancocuaresma.com/s/>. In this section we describe the contained data and their file formats.

5.1. Spectra

The library contains 78 spectra corresponding to the 34 benchmark stars. They cover the spectral range from 480 to 680 nm,

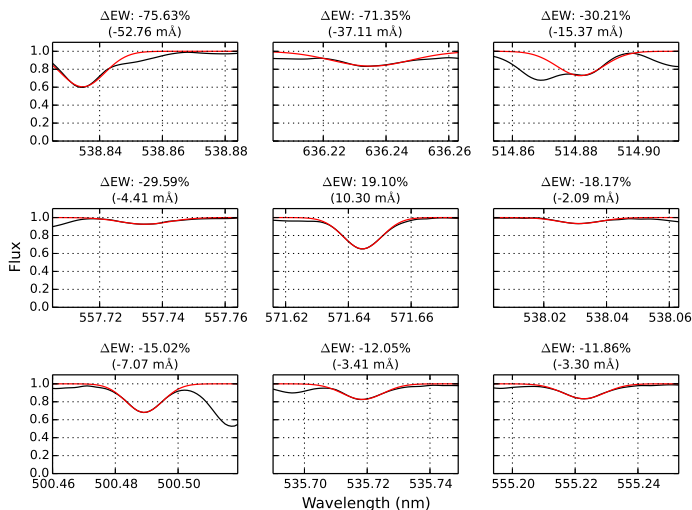


Fig. 7. Normalized fluxes (black) and fitted Gaussians (red) for the lines with the highest relative difference in EW compared to Ramírez & Allende Prieto (2011). The fluxes correspond to the Arcturus spectrum observed by NARVAL.

homogeneously sampled with wavelength step of 0.001 nm (equivalent to 190,000 bins).

We provide four library variants: convolved/not convolved original non-normalized fluxes and convolved/not convolved normalized spectra.

The spectra are saved in two different formats:

1. FITS format, following the standards of the IAU⁸ (Greisen & Calabretta 2002; Greisen et al. 2006), where the spectral coordinates (wavelengths) are specified in the header via CRVAL1 and CDELTA1 keywords. The FITS headers also contain metadata for each spectrum, such as their observation date, instrument, celestial coordinates, and history log. The fluxes and errors are stored, respectively, in the primary data unit and in an image extension (Grosbol et al. 1988) as 1D arrays.
2. Compressed plain text files with three columns delimited by tabulations: wavelength (nm), flux, and error.

5.2. Telluric lines

As described in Sect. 3.3, regions potentially affected by telluric lines were identified, thus the user can discard them easily. For each spectrum, we provide a plain text file with three columns (delimited by tabulations) which correspond to the telluric line peak, beginning, and end of the affected region (in nanometers).

5.2.1. Gap regions

As described in Sect. 3.4, some spectra contain gaps (regions without valid fluxes). We provide those regions in individual plain text files (one per spectrum) with two columns (delimited by tabulations), which correspond to the beginning and end of the gap (in nanometers).

6. Conclusions

We created a homogeneous library of high resolution and high S/N spectra corresponding to 34 benchmark stars with

Table 11. Relative EW differences with external measurements (Ramírez & Allende Prieto 2011; Luck & Heiter 2006, 2007).

Star	Instrument	ΔEW $\mu \pm \sigma$	Num. of lines
Sun	Atlas	0.01±0.07	107
Sun	HARPS	-0.03±0.07	101
Sun	NARVAL	-0.04±0.06	106
Sun	UVES	-0.04±0.08	94
Arcturus	Atlas	-0.02±0.12	109
Arcturus	HARPS	-0.05±0.12	104
Arcturus	NARVAL	-0.03±0.12	105
Arcturus	UVES	-0.02±0.12	101
Arcturus	UVES.POP	-0.03±0.12	100
18 Sco	HARPS	-0.02±0.15	866
18 Sco	NARVAL	0.00±0.15	885
δ Eri	HARPS	0.01±0.15	1071
δ Eri	NARVAL	0.01±0.15	1109
δ Eri	UVES	0.02±0.16	1055
δ Eri	UVES.POP	0.02±0.15	1072
β Gem	HARPS	0.02±0.16	1176
η Boo	HARPS	-0.04±0.14	562
η Boo	NARVAL	-0.04±0.14	564
HD 220009	HARPS	0.00±0.15	1048
HD 220009	NARVAL	-0.00±0.14	1075
Procyon	HARPS	-0.07±0.12	530
Procyon	NARVAL	-0.07±0.11	548
Procyon	UVES	-0.06±0.13	524
Procyon	UVES.POP	-0.05±0.12	526
61 Cyg A	NARVAL	0.04±0.23	717
61 Cyg B	NARVAL	0.12±0.31	764
Gmb 1830	NARVAL	0.06±0.21	414
μ Cas	NARVAL	-0.00±0.15	675
μ Leo	NARVAL	0.03±0.20	1041
Mean		-0.01±0.04	

four different variants (convolved/not convolved original non-normalized fluxes, convolved/not convolved normalized spectra). The library provides a powerful tool to assess spectral analysis methods and calibrate spectroscopic surveys.

We validated the consistency of the library by carefully checking the normalization and convolution treatments. The radial velocity corrections was certified by comparing the results with the high precision measurements of HARPS pipeline. We verified the coherence of the treated spectra by comparing them with EW measurements completely independent from our process. These strict tests proved the high quality level of the spectral library.

The whole creation and verification process was automated, minimizing human subjectivity and ensuring reproducibility. It also allows us to create new versions of the library adapted to particular needs (i.e., different resolutions and spectral ranges) of specific spectroscopic surveys or spectral analyses.

The Gaia FGK benchmark stars library provides an opportunity to homogenize spectroscopic results (from single observations to massive surveys), reducing their dispersion and making them more comparable. This higher level of homogeneity can lead to a better and more robust understanding of the Galaxy such as its formation, evolution, and current structure.

Acknowledgements. We thank N. Brouillet and T. Jacq for the help in the library construction. We also thank G. Sacco for the ingestion of our library in the second data release of the Gaia-ESO Survey. This work was partially supported by the Gaia Research for European Astronomy Training (GREAT-ITN)

⁸ International Astronomical Union

Marie Curie network, funded through the European Union Seventh Framework Programme [FP7/2007-2013] under grant agreement n. 264895. UH acknowledges support from the Swedish National Space Board (Rymdstyrelsen). The authors acknowledge the role of the SAM collaboration (<http://www.astro.uu.se/~ulrike/GaiaSAM>) in stimulating this research through regular workshops. Computer time for this study was provided by the computing facilities MClA (Mésocentre de Calcul Intensif Aquitain) of the Université de Bordeaux and of the Université de Pau et des Pays de l'Adour. All the software used in the data analysis were provided by the Open Source community.

References

- Allende Prieto, C. 2007, *AJ*, 134, 1843
- Allende Prieto, C., Majewski, S. R., Schiavon, R., et al. 2008a, *Astronomische Nachrichten*, 329, 1018
- Allende Prieto, C., Sivarani, T., Beers, T. C., et al. 2008b, *AJ*, 136, 2070
- Aurière, M. 2003, in *EAS Publications Series*, Vol. 9, *EAS Publications Series*, ed. J. Arnaud & N. Meunier, 105
- Ayres, T. R. 2010, *ApJS*, 187, 149
- Bagnulo, S., Jehin, E., Ledoux, C., et al. 2003, *The Messenger*, 114, 10
- Ballester, P., Modigliani, A., Boitquin, O., et al. 2000, *The Messenger*, 101, 31
- Baranne, A., Queloz, D., Mayor, M., et al. 1996, *A&AS*, 119, 373
- Bertaux, J. L., Lallement, R., Ferron, S., Boone, C., & Bodichon, R. 2013, *ArXiv e-prints*
- Blanco-Cuaresma, S., Soubiran, C., Jofré, P., & Heiter, U. 2013, *ArXiv e-prints*
- Dekker, H., D'Odorico, S., Kaufer, A., Delabre, B., & Kotzlowski, H. 2000, in *Society of Photo-Optical Instrumentation Engineers (SPIE) Conference Series*, Vol. 4008, *Society of Photo-Optical Instrumentation Engineers (SPIE) Conference Series*, ed. M. Iye & A. F. Moorwood, 534–545
- Donati, J., Semel, M., Carter, B. D., Rees, D. E., & Collier Cameron, A. 1997, *MNRAS*, 291, 658
- Freeman, K. C. 2010, in *Galaxies and their Masks*, ed. D. L. Block, K. C. Freeman, & I. Puerari, 319
- Gilmore, G., Randich, S., Asplund, M., et al. 2012, *The Messenger*, 147, 25
- Gray, R. O. & Corbally, C. J. 1994, *AJ*, 107, 742
- Greisen, E. W. & Calabretta, M. R. 2002, *A&A*, 395, 1061
- Greisen, E. W., Calabretta, M. R., Valdes, F. G., & Allen, S. L. 2006, *A&A*, 446, 747
- Grosbøl, P., Harten, R. H., Greisen, E. W., & Wells, D. C. 1988, *A&AS*, 73, 359
- Gustafsson, B., Edvardsson, B., Eriksson, K., et al. 2008, *A&A*, 486, 951
- Hinkle, K. & Wallace, L. 2005, in *Astronomical Society of the Pacific Conference Series*, Vol. 336, *Cosmic Abundances as Records of Stellar Evolution and Nucleosynthesis*, ed. T. G. Barnes, III & F. N. Bash, 321
- Hinkle, K., Wallace, L., Valenti, J., & Harmer, D. 2000, *Visible and Near Infrared Atlas of the Arcturus Spectrum 3727-9300 Å*
- Jofré, P., Heiter, U., Soubiran, C., et al. 2013, *ArXiv e-prints*
- Jofré, P., Panter, B., Hansen, C. J., & Weiss, A. 2010, *A&A*, 517, A57
- Katz, D., Soubiran, C., Cayrel, R., Adda, M., & Cautain, R. 1998, *A&A*, 338, 151
- Koleva, M., Prugniel, P., Bouchard, A., & Wu, Y. 2009, *A&A*, 501, 1269
- Kupka, F., Dubernet, M.-L., & VAMDC Collaboration. 2011, *Baltic Astronomy*, 20, 503
- Kurucz, R. L., Furenlid, I., Brault, J., & Testerman, L. 1984, *Solar flux atlas from 296 to 1300 nm*
- Lee, Y. S., Beers, T. C., Sivarani, T., et al. 2008, *AJ*, 136, 2022
- Luck, R. E. & Heiter, U. 2006, *AJ*, 131, 3069
- Luck, R. E. & Heiter, U. 2007, *AJ*, 133, 2464
- Magrini, L., Randich, S., Friel, E., et al. 2013, *A&A*, 558, A38
- Mayor, M., Pepe, F., Queloz, D., et al. 2003, *The Messenger*, 114, 20
- Molaro, P. & Monai, S. 2012, *A&A*, 544, A125
- Mucciarelli, A., Pancino, E., Lovisi, L., Ferraro, F. R., & Lapenna, E. 2013, *ApJ*, 766, 78
- Munari, U. & Sordo, R. 2005, *Memorie della Societa Astronomica Italiana Supplementi*, 8, 170
- Pepe, F., Mayor, M., Galland, F., et al. 2002, *A&A*, 388, 632
- Percival, S. M., Salaris, M., Cassisi, S., & Pietrinferni, A. 2009, *ApJ*, 690, 427
- Perryman, M. A. C., de Boer, K. S., Gilmore, G., et al. 2001, *A&A*, 369, 339
- Posbic, H., Katz, D., Caffau, E., et al. 2012, *A&A*, 544, A154
- Prugniel, P. & Soubiran, C. 2001, *A&A*, 369, 1048
- Ramírez, I. & Allende Prieto, C. 2011, *ApJ*, 743, 135
- Recio-Blanco, A., Bijaoui, A., & de Laverny, P. 2006, *MNRAS*, 370, 141
- Sánchez-Blázquez, P., Peletier, R. F., Jiménez-Vicente, J., et al. 2006, *MNRAS*, 371, 703
- Steinmetz, M., Zwitter, T., Siebert, A., et al. 2006, *AJ*, 132, 1645
- Thévenin, F., Kervella, P., Pichon, B., et al. 2005, *A&A*, 436, 253
- Valdes, F., Gupta, R., Rose, J. A., Singh, H. P., & Bell, D. J. 2004, *ApJS*, 152, 251
- Valenti, J. A. & Piskunov, N. 1996, *A&AS*, 118, 595
- Vazdekis, A., Ricciardelli, E., Cenarro, A. J., et al. 2012, *MNRAS*, 424, 157
- Wu, Y., Luo, A.-L., Li, H.-N., et al. 2011, *Research in Astronomy and Astrophysics*, 11, 924
- York, D. G., Adelman, J., Anderson, Jr., J. E., et al. 2000, *AJ*, 120, 1579
- Zhang, F., Li, L., & Han, Z. 2005, *MNRAS*, 364, 503
- Zhao, G., Chen, Y.-Q., Shi, J.-R., et al. 2006, *CJAA*, 6, 265
- Zucker, S. 2003, *MNRAS*, 342, 1291